Polymer 51 (2010) 807–815

Contents lists available at ScienceDirect

Polymer

journal homepage: www.elsevier.com/locate/polymer

Crystallization kinetics and crystalline structure of biodegradable Poly(ethylene adipate)

Jinjun Yang, Pengju Pan, Tungalag Dong, Yoshio Inoue*

Department of Biomolecular Engineering, Tokyo Institute of Technology, 4259-B-55 Nagatsuta, Midori-ku, Yokohama 226-8501, Japan

ARTICLE INFO

Article history:
Received 26 September 2009
Received in revised form
26 November 2009
Accepted 29 November 2009
Available online 4 December 2009

Keywords:
Crystallization kinetics
Crystalline structure
Poly(ethylene adipate)

ABSTRACT

The crystallization kinetics, morphology and crystalline structure of biodegradable poly(ethylene adipate) (PEA) with high and low molecular weights (HMW, LMW) were systematically investigated. The crystallization kinetics obtained from differential scanning calorimetry analysis indicated that both the primary and secondary crystallizations occur during the isothermal and non-isothermal crystallization processes for HMW and LMW PEA samples. Under the same crystallization condition, LMW PEA was found to crystallize faster than HMW PEA. The PEA sample forming the ring-band spherulite presents a higher Avrami exponent value (n) than that without the ring-band spherulite, due in part to the different crystal growth mechanism. From the results of wide angle X-ray diffraction and Fourier transform infrared spectroscopy, it was confirmed that the crystalline structure of PEA is not dependent on the crystallization temperature (T_c) and MW. From the in-situ FTIR investigation of the crystallization kinetics, it is concluded that, during the isothermal crystallization process at 42 °C, the structural rearrangement of the ester group precedes that of the C–C backbone.

1. Introduction

Over the past several decades, much attention has been paid to biodegradable polymers that are considered as green, environment-friendly, and biocompatible materials [1]. Aliphatic polyester is a kind of typical biodegradable polymer. They are susceptible to hydrolytic or enzymatic degradation in natural environments and also have comparable physical properties to many traditional thermoplastics [1]. Many final products have been developed from these polymers and used for disposable plastic bags, films and matrix resins for biomedical materials and drug carriers [2–4]. The aliphatic polyester prepared from glycol and diacid by polycondensation is a kind of promising biodegradable material which has been attracting considerable attention in recent years [1]. Poly(butylene succinate) (PBS) and poly(butylene succinate-*co*-adipate) (PBSA) have been commercialized under the trademark of BIONOLLE® [1].

Poly(ethylene adipate) (PEA) is a kind of aliphatic polyester made from glycol and diacid, which presents the nature of biodegradability. It has a similar chemical structure to that of poly(butylene adipate) (PBA), but bears the different number of methylene unit (4 CH_2) from that of PBA (6 CH_2). PBA has been reported to show two types of crystalline forms, denoted as α-form ($T_c \geq 32$ °C) and β-form crystal ($T_c \leq 28$ °C) [5–8], during the crystallization at different temperatures. The effect of crystallization condition on the crystalline structure of PEA is unclear. At present, two suggestions have been reported on the temperature-dependent crystalline structure of PEA. Some researchers [9–11] argued that it shows only one crystal modification that is packed in a monoclinic unit cell with the dimensions of $a = 0.547$ nm, $b = 0.723$ nm, and c (fiber axis) $= 1.172$ nm, and the monoclinic angle of $\alpha = 113.5°$. On the other hand, Satoh and coworkers [12] have recently reported that the plot of spherulite growth rate (G) against T_c for PEA shows two peaks, instead of the typical bell-shape curve. This discontinuousness in spherulite growth rate or the peculiar crystallization kinetics of PEA is very similar to those of many polymorphic polymers, such as PBA [8], poly(3-hydroxypropionate) (PHP) [13], and poly(L-lactide) (PLLA) [14], in which the different crystal modifications show the peculiar G vs T_c plots. This may be an indication of polymorphic crystallization. Satoh et al. have suggested that PEA shows two types crystals named as α- and β-crystal and further proposed that the PEA β-form crystal is packed in an orthorhombic unit cell with the dimensions of $a = 0.512$ nm, $b = 0.841$ nm, and c (fiber axis) $= 1.228$ nm [12]. In addition, in a specific T_c range, PEA shows the interesting ring-band spherulite during the isothermal crystallization process, rather than the usual Maltese-cross one [11,15], which also occurs for the polymorphic PBA [16]. Moreover, it has been pointed out that the multiple melting peaks (3–4 peaks) appear in the heating curves for

* Corresponding author. Tel.: +81 45 924 5794; fax: +81 45 924 5827.
E-mail address: inoue.y.af@m.titech.ac.jp (Y. Inoue).

0032-3861/$ – see front matter © 2009 Elsevier Ltd. All rights reserved.
doi:10.1016/j.polymer.2009.11.065

PEA isothermally melt-crystallized at various temperatures [11]. The multiple melting behavior of polymer is generally resulted by the different crystalline phases or the melt-recrystallization-remelt mechanism. Woo et al. [11] have argued that these multiple melting peaks are associated with the melt-recrystallization-remelt mechanism, but not the melting of different crystalline phases. Considering the above interesting phenomena and different opinions concerning the crystallization behavior of PEA, the T_c-dependent crystalline structure for PEA need to be further investigated. Since the physical, mechanical properties and biodegradability of biodegradable polymers are quite dependent on their crystalline structure [17], it is of fundamental importance to clarify the relationships between crystalline structure and crystallization conditions of PEA for its industrial applications.

So far, the reports on the comprehensive and detailed analysis of the crystallization kinetics of PEA are very limited. It is well known that the crystallization process greatly affects the crystalline structure, morphology, mechanical and physical properties and biodegradation of polymer [2,18–21]. The crystallization kinetic is also a very key factor to the processing and modeling of semi-crystalline thermoplastics. In order to control and to adjust crystallization rate and the degree of crystallinity and to get the desired morphology and properties, the study on the crystallization kinetics of PEA is considered to be important.

It is reported that the molecular weight is also one of important factors influencing crystalline structure because polymers with different molecular weights (MWs), such as nylon-6 [22] and PHP [13], frequently present different thermodynamic parameters and crystallization kinetics. When melt-crystallized at relatively low temperature, the low molecular weight (LMW) nylon-6 mainly forms the more stable α-crystal, but high molecular weight (HMW) one predominantly develops the unstable γ-form crystal. The LMW PHP sample only produces δ–form crystal, which can not be found in HMW one. Accordingly, both the HMW and LMW PEAs are used for study on the crystallization kinetic and crystalline structure in this work.

Fourier transform infrared (FTIR) spectrometry has been widely used to analyze the structural evolution and/or kinetics of polymeric materials [23–25]. It is well documented that FTIR spectroscopy is highly sensitive to the conformation and other subtle structural changes of the polymer chains, for example, the change of chain packing in the crystalline phase [26,27]. The structural development of chain segment is usually detected by in-situ observation of the IR characteristic bands [26,27]. FTIR spectroscopy can also be applied to explore variations in the intra- and intermolecular interactions and structural evolution of macromolecules at the molecular level during the melting or crystallization process, for its sensitivity to the conformation and local molecular environment of macromolecule. FTIR spectra of many kinds of biodegradable polymers have been analyzed and their characteristic bands for different phases have been assigned [26–33]. To the best of our knowledge, the detailed study on the crystalline structure of PEA by FTIR spectrometry has not been reported.

In this work, the morphology of PEA was observed by polarized optical microscopy (POM). The crystallization kinetics of HMW and LMW PEAs under the isothermal and non-isothermal crystallization conditions were investigated in depth by DSC. In addition, the T_c- and MW-dependent crystalline structures were also analyzed in detail by WAXD and FTIR.

2. Experimental

2.1. Materials

HMW ($M_w = 10{,}000$ Da) and LMW PEA ($M_w = 1000$ Da) samples were purchased from Aldrich Chemical Corporation. Before use, they were firstly purified by precipitating into ethanol from the chloroform solution. After being isolated by ultracentrifugation, they were dried completely in the vacuum oven at 40 °C for 1 week.

2.2. Measurements

2.2.1. Differential scanning calorimetry (DSC)

The thermal behaviors of HMW and LMW PEAs were measured by a Pyris Diamond DSC instrument (Perkin-Elmer Japan Co., Tokyo, Japan) equipped with a Perkin-Elmer intracooler 2P cooling accessory. The temperature and heat flow at different heating rates were calibrated using an indium standard with nitrogen purging. For the isothermal crystallization process, the PEA samples (5–8 mg) were melted to 80 °C for 2 min to eliminate the previous thermal history. Then, they were quenched quickly at a rate of 100 °C/min to the desired T_cs. After the completion of crystallization, the samples were reheated to 80 °C at a heating rate of 10 °C/min. For the non-isothermal crystallization process, the PEA samples were firstly melted to 80 °C for 2 min, then cooled to −50 °C at the selected cooling rates. After the completion of crystallization, the samples were also reheated to 80 °C at a heating rate of 10 °C/min.

2.2.2. Polarized optical microscopy (POM)

POM observation was performed on a BX90 microscopy (Olympus Co., Tokyo, Japan) equipped with a digital camera. The sample was sandwiched between two glass slides, and melted at 80 °C for 2 min in a LK-600 hot stage (Linkam Scientific Instrument). During melting, the sample was pressed slightly to form a thin film with a thickness of ≈0.1 mm. Then, it was quickly transferred to another hot stage (Mettler FP82HT) preset to the desired T_cs. The photographs were recorded after the completion of crystallization.

2.2.3. Wide angle X-ray diffraction (WAXD)

The PEA samples sandwiched between two iron plates with the thickness of 2 mm were pressed for 2 min at 80 °C under 5 MPa on the hot press (TOYOSEIKI Co., Tokyo, Japan). Then the pressed sample films were quickly threw into the water bath preset to the desired T_cs. After the completion of isothermal crystallization, the PEA films were measured at room temperature by WAXD. For the PBA sample quenched into the liquid nitrogen from 80 °C, after dipping in the liquid nitrogen for 3 min, it was taken out and annealed at the room temperature for 30 min for the cold crystallization. The WAXD patterns were recorded on a Rigaku RU-200 with Ni-filtered CuKα radiation ($\lambda = 0.1542$ nm), worked at 40 kv and 200 mA (Rigaku Corp., Tokyo, Japan). The WAXD patterns were collected in the range of Bragg angles 5–50° at a scanning rate of 1°/min.

2.2.4. Fourier Transform Infrared (FTIR) spectroscopy

The transmission FTIR measurements were carried out on an AIM-8800 automatic infrared microscope (Shimadzu Corp., Kyoto, Japan). The samples were sandwiched between 2 pieces of BaF_2 slides. The samples for FTIR measurements were prepared as follows. The samples were firstly heated to 80 °C and held for 2 min to remove the thermal history on a Linkam-600 hot stage (Japan High Tech Co., Ltd. Fukuoka, Japan). Then, they were quickly transferred to the other hot stage preset to the desired T_cs for isothermal crystallization. In order to avoid the temperature variation and thermal lag as far as possible, the hot stage is connected with a set of cooling equipment with liquid nitrogen. After the completion of crystallization, the samples were analyzed by FTIR. To avoid the effect of the temperature on FTIR spectra, these IR spectra were collected at 20 °C. For the isothermal crystallization at 42 °C, time-resolved IR spectroscopy was employed and each

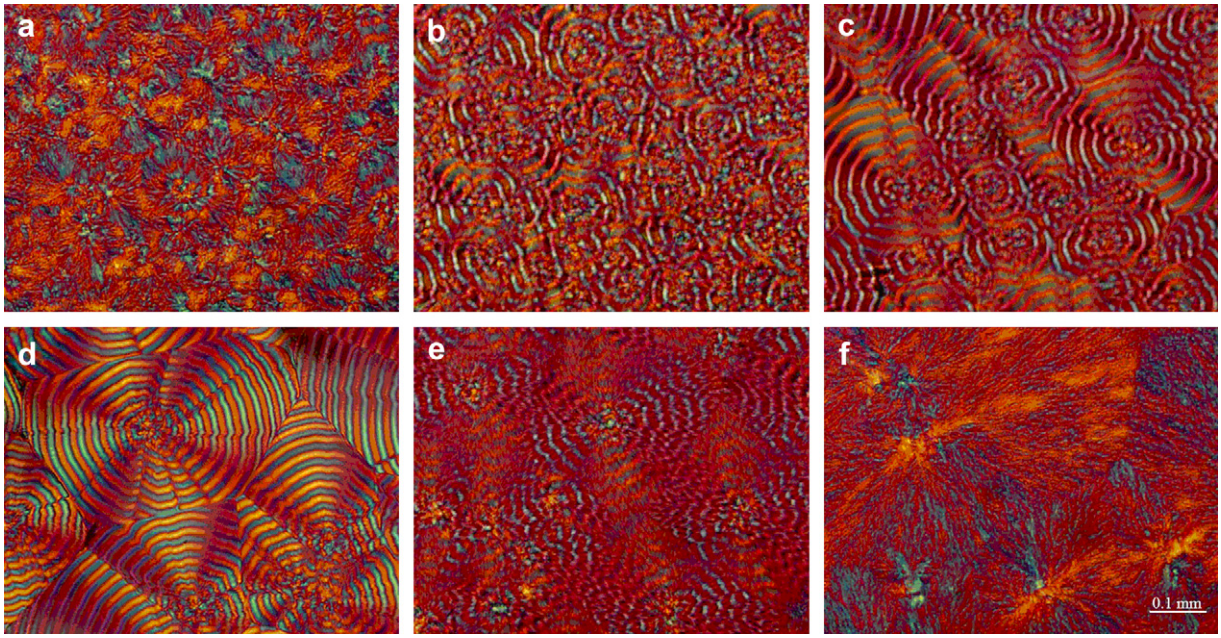

Fig. 1. POM micrographs of HMW PEA melt-crystallized at (a) 26, (b) 27, (c) 30, (d) 32, (e) 34 and (f) 35 °C, respectively.

spectrum was recorded with the time interval of 3 min. All the FTIR spectra were collected at an accumulation of 32 scans and a resolution of 2 cm^{-1}.

3. Results and discussion

3.1. Spherulitic morphology observation by POM

In Fig. 1 are shown the POM micrographs of the HMW PEA melt-crystallized at various temperatures. It can be clearly observed that the typical Maltese-cross patterns appear at $T_c = 26$ and 35 °C (a and f in Fig. 1). Both the spherulite density and spherulite number of PEA melt-crystallized at 26 °C are greater than those melt-crystallized at 35 °C. At $T_c = 27$–34 °C (b–e in Fig. 1), the ring-band spherulite can be discerned, though a small amount of Maltese-cross spherulite can also be found in the PEA sample melt-crystallized at 27 °C. The very clear ring-band spherulite appears at $T_c = 32$ °C. The ring-band spherulite of the LMW PEA can also be observed at $T_c = 27$–35 °C (data not shown).

This interesting phenomenon is similar to the results reported by other researchers [34,35]. It is reported that the formation of ring-band spherulite is probably attributed to the following two interpretations. Firstly, it is ascribed to the cooperative lamellar twisting in the direction of radial growth. Secondly, it is strongly related to the structural discontinousness resulted from the periodical growth of crystal [35]. The former one is widely accepted. The unbalanced stress on the lamellar surface is considered as the driving force of lamellar twisting and the distances in ring bands are associated with mobility of polymer chain segments [35].

3.2. Analysis of crystallization kinetics by DSC

3.2.1. Isothermal crystallization kinetics

The DSC crystallization curves for the HMW and LMW PEAs at various temperatures are shown in Fig. 2. It can be observed that the crystallization time becomes longer and the exothermic peak becomes broader with increasing T_c. At the same T_c, the LMW PEA needs the shorter time to finish the crystallization than the HMW PEA, suggesting that the LMW PEA is easier to crystallize than the HMW PEA.

The Avrami equation is the most simple and widely accepted method to analyze the crystallization kinetics of polymers [2,18–21,36]. The Avrami equation can be expressed as follows.

$$\log[-\ln(1-X_t)] = n\log t + \log k \quad (1)$$

where t and X_t are the crystallization time and the relative crystallinity at time t. n is Avrami exponent and k represents the

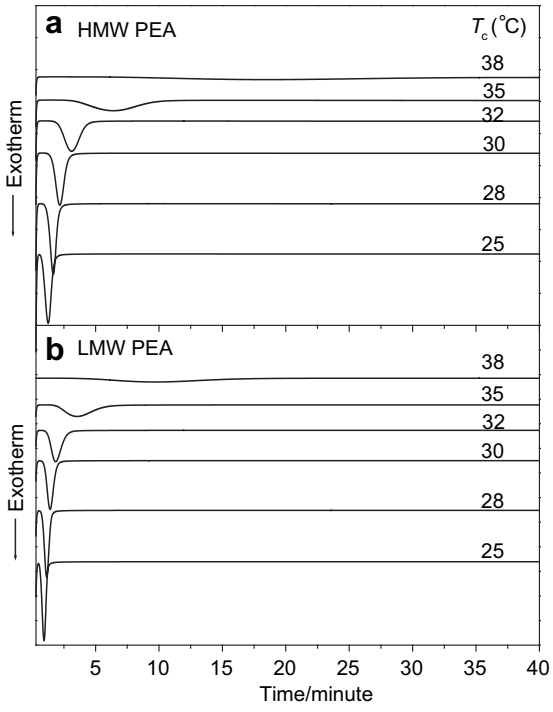

Fig. 2. DSC curves for (a) HMW and (b) LMW PEAs isothermally crystallized at various temperatures.

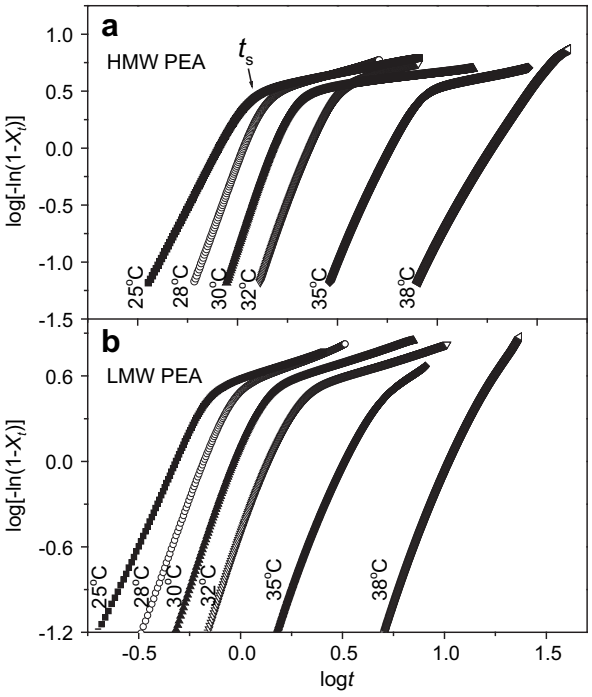

Fig. 3. Avrami plots of log[−ln(1 − X_t)] versus logt at various crystallization temperatures for (a) HMW and (b) LMW PEA.

crystallization rate constant. The crystallization half time ($t_{1/2}$) is also a frequently used parameter, which is defined as the time where the relative crystallinity reaches to the half of the complete crystallization. $t_{1/2}$ can be obtained by equation (2).

$$t_{1/2} = (\ln 2/k)^{1/n} \tag{2}$$

The plots of log[−ln(1 − X_t)] versus log$t$ at the different temperatures during the isothermal crystallization process for HMW and LMW PEAs are presented in Fig. 3. Most of the curves shown in Fig. 3 are not linear, even though for the curve of LMW PEA samples melt-crystallized at 38 °C, also showing a slight deviation in the later stage of crystallization. It has been reported that the primary crystallization processes of many polymers are accompanied by the secondary crystallization and several methods have been proposed to determine the onset time of the secondary crystallization [2,37–40]. The secondary crystallization is mainly referred to the later stage of crystallization, which occurs within the interlamellar or interfibrillar region and is rejected or trapped between the interfibrillar structure [2,20,37–42]. The simplest method is referred to the time (t_s) where the discontinuity of the plot of log[−ln(1 − X_t)] versus log$t$ takes place [2,40]. These curves shown in Fig. 3 are composed of two linear parts, indicating that the primary crystallization is accompanied by the secondary crystallization. It seems that the plots corresponding to lower T_cs show more distinct deviation than those at higher T_cs, suggesting that the species melt-crystallized at higher temperatures can crystallize more completely to form more perfect crystal in the crystallization process.

As depicted in Fig. 3, the primary and secondary crystallization processes take place continuously and were separated at t_s. So the kinetics in both the primary and secondary crystallization can be investigated separately. The isothermal crystallization kinetic parameters for the HMW and LMW PEAs are listed in Table 1.

From Table 1, it can be found that during the primary crystallization of HMW PEA, with increasing T_c, the values of $t_{1/2}$ and the crystallization exotherm (ΔH) increase, while that of k decreases. It is notable that the Avrami exponent n for the HMW PEA melt-crystallized at 28, 30 and 32 °C (from 4.09 to 4.67) is higher than the counterparts melt-crystallized at 25, 35 and 38 °C (between 2.87 and 3.22). It has been reported that n is influenced not only by the crystal growth direction (one-, two- or three-dimensional growth) but also by the crystal morphology [2]. Based on the above POM result, the PEA samples melt-crystallized at T_c = 27–34 °C form the ring-band spherulites, which is different from the Maltese-cross spherulites developed at $T_c \leq 26$ °C or ≥ 35 °C. It is suggested that the ring extinction in the PEA ring-band spherulite is caused by the regular lamellar twisting and the twisting period corresponds to the distance between two equivalent birefringent rings, indicating the existence of two equivalent chain tilting positions with zero birefringence in one twisting period [34]. It is probably the different crystal growth mechanism why the values of n of PEA melt-crystallized at 28–32 °C are different from those melt-crystallized at low (e.g., 25 °C) or high (35 and 38 °C) T_cs.

It is well known that the secondary crystallization takes place in the later stage of crystallization. As described above, it occurs in the confined or restricted space, such as interfibrillar and/or interlamellar region, and the crystal can not grows freely ($n \leq 1$). Thus, the Avrami exponent n in the secondary crystallization is much lower than that in the primary crystallization. Expected results can be found for the LMW PEA, as shown in Table 1. With comparison of the data for the HMW and LMW PEA, it can be found that during the primary crystallization process, at the same crystallization temperature, the values of $t_{1/2}$ are lower and those of k are higher for the LMW PEA than the counterparts for the HMW PEA. It further indicates that the LMW PEA is easier to crystallize than the HMW PEA under the same crystallization conditions.

3.2.2. Non-isothermal crystallization kinetics

Up to date, various methods have been proposed to clarify the non-isothermal crystallization process, i.e. Tobin, Malkin, and Urbanovici-Segal macrokinetic models [20]. However, considering the various influencing factors, such as cooling rate, thermal

Table 1
Isothermal crystallization kinetic parameters for HMW and LMW PEAs.

	HMW PEA						LMW PEA					
	Primary crystallization				Secondary crystallization		Primary crystallization				Secondary crystallization	
T_c (°C)	$t_{1/2}$ (min)	ΔH (J/g)	n	k (min^{-1})	n	k (min^{-1})	$t_{1/2}$ (min)	ΔH (J/g)	n	k (min^{-1})	n	k (min^{-1})
25	0.74	−56.4	3.22	1.87	0.56	0.58	0.43	−53.9	3.09	9.15	0.49	0.72
28	1.01	−58.1	4.29	0.66	0.65	0.47	0.61	−56.2	4.08	3.97	0.58	0.69
30	1.44	−59.1	4.27	0.13	0.71	0.08	0.87	−57.3	4.16	1.14	0.48	0.55
32	2.17	−61.5	4.35	0.029	0.64	0.017	1.29	−59.7	4.31	0.29	0.46	0.13
35	5.44	−63.3	3.08	0.0023	0.68	0.0016	3.01	−60.5	2.93	0.027	0.75	0.011
38	17.48	−66.7	2.87	0.00019	N.S.[a]	N.S.[a]	9.63	−63.1	3.19	0.00051	0.83	0.00032

[a] No secondary crystallization can be observed.

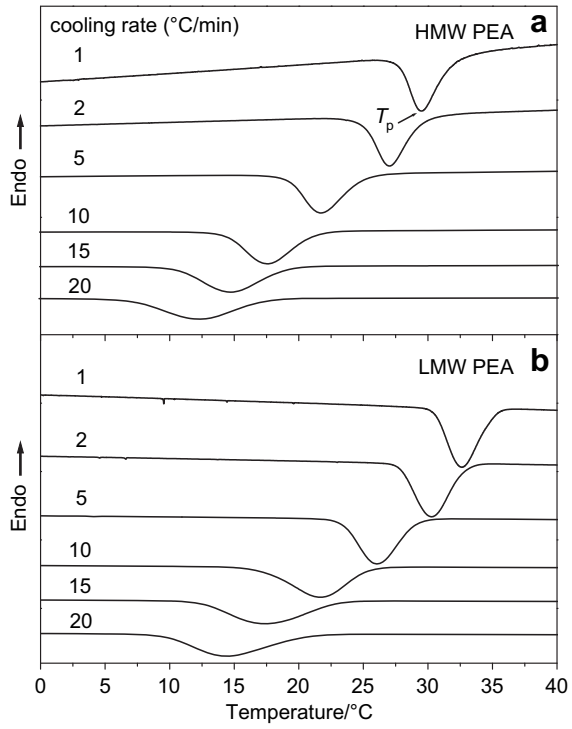

Fig. 4. Non-isothermal crystallization curves of (a) HMW and (b) LMW PEAs at the cooling rate of 10 °C/min from 80 °C.

gradient, and so on, it is very difficult to describe precisely and comprehensively the non-isothermal crystallization process with only a kind of method mentioned above. Here, the Avrami equation is still employed to analyze the non-isothermal crystallization. In this case, the crystallization time t is defined as $(T_0 - T_t)/\alpha$, where T_0 and T_t denote respectively the onset temperature and the randomly chosen temperature during the non-isothermal crystallization process, and α refers to the cooling rate.

Fig. 4 depicts the DSC non-isothermal crystallization curves at various cooling rates of (a) HMW and (b) LMW PEAs plotted against the temperature. With increasing the cooling rate, the crystallization peak (T_p, denoted as the arrow) shifts to lower temperature region and becomes broader. At the same cooling rate, T_p of the LMW PEA is higher than that of the HMW PEA, further indicating that the LMW PEA crystallizes more easily than the HMW PEA. The plots of $\log[-\ln(1 - X_t)]$ versus $\log t$ during the non-isothermal crystallization process for the HMW and LMW PEAs are also analyzed (data not shown). The primary and secondary crystallization can also be observed in the plots of $\log[-\ln(1 - X_t)]$ versus $\log t$ because these patterns are not linear yet. It should be pointed out that higher the cooling rate is, more severe the deviation of the pattern is. It indicates that the high cooling rate is unfavorable for the complete crystallization, as there is not enough time to adjust PEA chain structure in the crystalline lattice.

The corresponding crystallization parameters are listed in Table 2. With increasing the cooling rate, the value of $t_{1/2}$ decreases, while that of k increases. So the high cooling rate increases the crystallization rate. It is interesting to note that the n values for the cooling rate of 1 and 2 °C/min are higher than those in other cases for the HMW PEA sample. The DSC curves at the cooling rate of 1 and 2 °C/min show the crystallization peaks at 29.5 and 27.1 °C, respectively. That is to say, the predominant crystallization occurs at the above two temperatures at which the ring-band spherulites form. Different crystal morphologies result in different values of n. The same result is also found for the LMW PEA (in the cooling process at the cooling rate of 1 and 2 °C/min). Similarly, the n value in the secondary crystallization is significantly lower than that in the corresponding primary crystallization because the former occurs in the confined region.

3.3. Analysis of crystalline structure by WAXD

As mentioned in Introduction part, it is still a controversial topic on the crystalline structure of PEA. No convincing evidence has been provided and no clear conclusion has been drawn for its crystalline structure until now. Generally, polymer with polymorphism shows different WAXD peaks which are attributed to different crystalline phases. Temperature-dependent polymorphism in many biodegradable polyesters are frequently found, i.e., PBA [5–8], PLLA [14,41], and so on. Here, WAXD was employed to study the crystalline structure of PEA melt-crystallized at different temperatures.

Fig. 5 shows the WAXD patterns with 2θ ranging from 19 to 28° for the HMW and LMW PEAs melt-crystallized in a wide temperature range (0–40 °C) and quenched into the liquid nitrogen. Here, the PEA sample quenched to the liquid nitrogen from the melt state is presented only for the comparison. As shown in Fig. 5(a), all these five WAXD curves of HMW PEA present 3 distinct reflection peaks locating at 20.5, 21.7 and 24.6°, corresponding to (111), (110) and (020) reflection planes, respectively [42,43]. In addition, a weak shoulder peak situates at the right side of peak (020). However, for the HMW PEA, two interesting points can be observed. With an increase in T_c, the intensity of peak (111) decreases significantly. Especially at 40 °C, the peak (111) is very weak in intensity. In addition, the shoulder peak gradually depresses in the intensity with T_c and disappears at $T_c = 40$ °C. This interesting phenomenon is probably associated with the orientation of HMW PEA spherulites in the film plane and the very large spherulites are formed at high T_c (with a diameter of about 1 mm at 40 °C, data not shown) which can greatly influence the orientation of HMW PEA spherulite since the spherulite size of HMW PEA is highly dependent on T_c. That is to say, the huge spherulite for the HMW PEA is subjected to the large orientation during the crystallization of film plane. For the LMW PEA sample, because of the faster crystallization rate, the

Table 2
Non-isothermal crystallization kinetic parameters for HMW and LMW PEAs.

	HMW PEA							LMW PEA						
	Primary crystallizaiton					Secondary crystallization		Primary crystallization					Secondary crystallization	
α (°C/min)	T_p (°C)	$t_{1/2}$ (min)	ΔH (J/g)	n	k (min^{-1})	n	k (min^{-1})	T_p (°C)	$t_{1/2}$ (min)	ΔH (J/g)	n	k (min^{-1})	n	k (min^{-1})
1	29.5	5.19	−60.5	4.51	0.00022	0.67	0.00013	32.6	5.08	−58.1	4.38	0.00039	0.79	0.00027
2	27.1	3.93	−58.3	4.17	0.0018	0.71	0.0011	30.3	3.36	−56.4	4.21	0.0057	0.81	0.0041
5	21.9	1.62	−57.1	2.89	0.041	0.73	0.024	26.1	1.51	−55.8	3.18	0.083	0.84	0.069
10	17.7	1.03	−55.4	2.91	0.56	0.69	0.29	21.7	0.87	−54.2	2.92	1.31	0.76	0.38
15	14.8	0.75	−54.2	2.78	3.45	0.75	0.38	17.4	0.71	−52.7	2.89	5.76	0.68	0.51
20	12.3	0.64	−53.3	3.01	7.29	0.73	0.67	14.3	0.61	−51.9	2.96	10.51	0.71	0.72

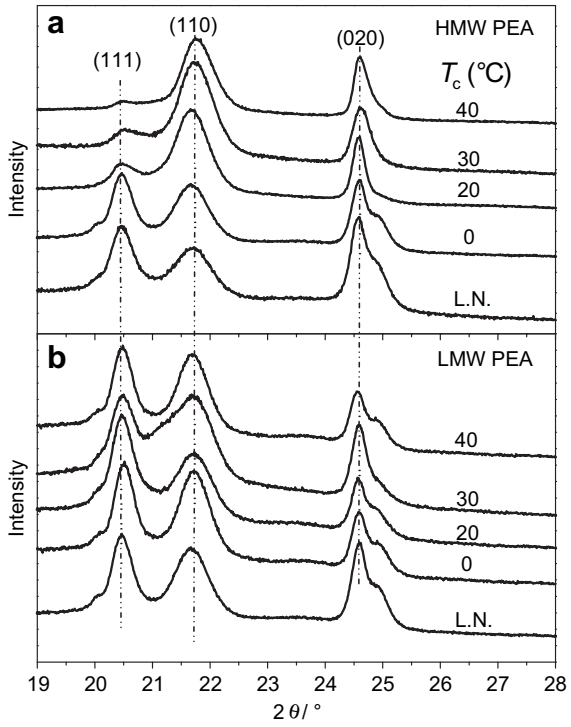

Fig. 5. WAXD patterns of (a) HMW and (b) LMW PEAs melt-crystallized at various temperatures. L.N. represents the sample quenched in liquid nitrogen from melting state.

spherulites with smaller size and the greater density are found at all T_cs, which affect little the orientation of LMW PEA spherulite. So the intensities of the peak (111) and the shoulder peak in the WAXD patterns for the HMW PEA sample change dramatically with T_c. This phenomenon is similar to the result for poly[(3-hydroxybutyrate)-*co*-(3-hydroxyhexanoate)] (PHBHHx) and poly(3-hydroxybutyrate) (PHB) [36,44]. It has been reported that the intensity of (110) peak for the neat PHBHHx decreases significantly with an increase in T_c. From the above WAXD results, it is concluded that the crystalline structure of PEA is not dependent on T_c and MW.

3.4. Analysis of crystalline structure by FTIR

The finger print region in the FTIR spectrum, i.e., 1500–900 cm^{-1}, is usually sensitive to the crystallization and melting processes of aliphatic polyester [13]. The IR spectra in the finger print region for HMW and LMW PEA sample melt-crystallized at various temperatures are shown in Fig. 6. Many IR bands are presented for the comparison between HMW and LMW PEA. Almost no distinct difference can be discerned for the IR spectra of HMW and LMW PEA in Fig. 6 (a) and (b).

Here, the HMW PEA was chosen to study the effects of crystallization conditions on their FTIR spectra. For clarity, the finger print region is divided into three wavenumber regions, that is, 1500–1300, 1300–1100, and 1100–900 cm^{-1}, respectively. Moreover, the corresponding second derivatives are presented to show the more subtle differences in Figs. 7–9.

Based on the previous reports on FTIR spectra of polyesters [14,45,46], FTIR bands of PEA can be assigned as follows. The vibration bands in the range of 1500–1400 cm^{-1} are attributed to the CH_2 bending mode and those in the region between 1400 and 1300 cm^{-1} are related to the CH_2 wagging mode. The bands from 1300 to 1100 cm^{-1} are assigned to the coupling of the asymmetric stretching and symmetric stretching mode for the C–O–C group. The bands which situate between 1100 and 1000 cm^{-1} are associated with the C–C stretching mode. The IR bands in the range of 1000–900 cm^{-1} are assigned to the CH_2 rocking mode.

Fig. 7 depicts (a) the IR spectra and (b) the corresponding second derivatives ranging from 1500 to 1300 cm^{-1} for the HMW PEA melt-crystallized at various temperatures. The main absorption bands, such as the 1467, 1459, 1437, 1422, 1411 and 1388 cm^{-1} bands appear. Almost no difference can be observed for these major IR bands of the samples even crystallized at different temperatures. Furthermore, the corresponding second derivatives also show almost the same peaks and peak positions among these samples. Two doublet bands (band-splitting) can be identified, i.e., the 1467 and 1459 cm^{-1} bands, and the 1422 and 1411 cm^{-1} bands, which are ascribed to the CH_2 asymmetrical bending mode $\delta_{as}(CH_2)$ and the CH_2 symmetrical bending mode $\delta_s(CH_2)$, respectively. In addition, the 1437 cm^{-1} band is attributable to the $\delta_s(CH_2)$ mode and the 1388 cm^{-1} one to the asymmetrical wagging mode $\sigma_{as}(CH_2)$.

The IR spectra and the corresponding second derivatives ranging from 1300 to 1100 cm^{-1} are shown in Fig. 8. In this region, the 1281, 1276, 1258, 1166 and 1162 cm^{-1} bands are observed. The 1281, 1276 and 1258 cm^{-1} bands are associated with the C–O–C asymmetrical stretching mode ν_{as}(C–O–C) and the 1166 and 1162 cm^{-1} bands are ascribed to the C–O–C symmetrical stretching mode ν_s(C–O–C), respectively. Two interesting features should be addressed. The band-splitting (the 1281 and 1276 cm^{-1} bands) only can be discerned for theses three IR spectra of the PEA sample melt-crystallized at 30, 32 and 33 °C (denoted as the arrow in Fig. 8 (a)), while no band-splitting can be observed in other cases. On the other hand, only the 1162 cm^{-1} band can be found in the IR spectra of PEA melt-crystallized at 0, 20 and 40 °C, but the corresponding band for the PEA sample melt-crystallized at 30, 32, 33 °C shifts to the higher wavenumber region, 1166 cm^{-1}.

As aforementioned, the ring-band spherulite only appears in the PEA sample melt-crystallized at the temperature of 27–34 °C. That is, only the band-splitting can be found in the IR spectra of the PEA

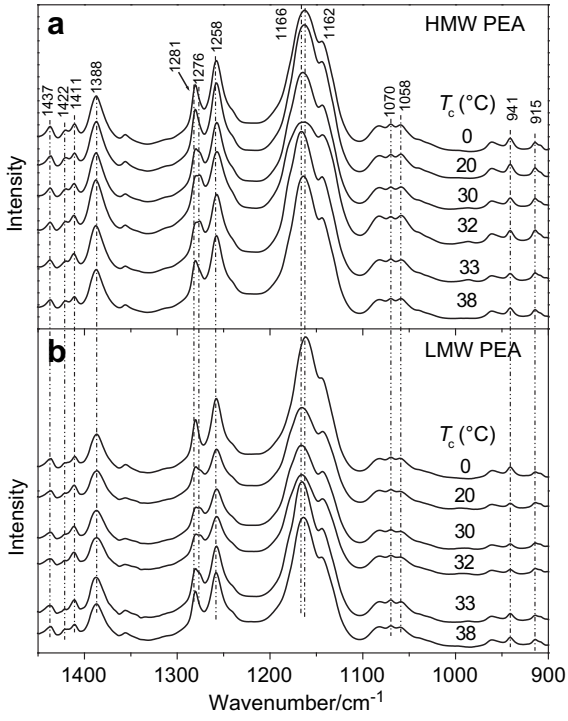

Fig. 6. IR spectra for (a) HMW and (b) LMW PEA melt-crystallized at various temperatures.

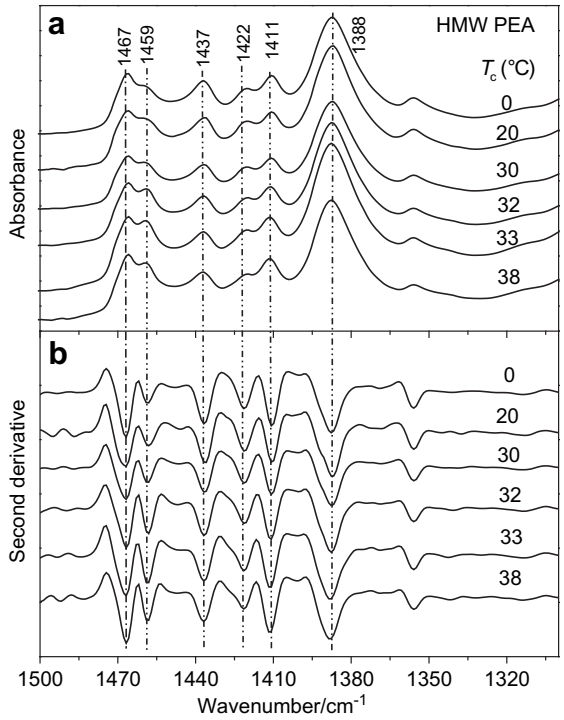

Fig. 7. (a) FTIR spectra and (b) the corresponding second derivatives in the wavenumber region of 1500–1300 cm^{-1} for HMW PEA melt-crystallized at various temperatures.

sample with the ring-band spherulite. When the crystallization temperature is in the range of 27–34 °C, the 1162 cm^{-1} band in the IR spectra of the PEA sample with no ring-band spherulite shifts to 1166 cm^{-1}. Therefore, the wavenumber shift and band-splitting are probably caused by the unique ring-band spherulite which is attributed to the lamellar twisting during the spherulite growth process. The lamellar twisting in the growth process undoubtedly and significantly affects the interaction between the C–O–C groups of the adjacent chain.

According to our previous study [46], the band-splitting appeared at 1485 and 1477 cm^{-1} in PBA was only observed in the β–form, which shows the stronger interaction between the adjacent chains within crystalline phase. In the case of PEA, the band-splitting is probably ascribed to the stronger interaction of C–O–C between the adjacent crystalline molecules during the lamellar twisting process. It is pointed out [27] that the bands in the region of 1300–1100 cm^{-1} associated with the C–O–C vibration in PBA are very sensitive to the annealing time. That is, the detectable changes in the IR bands reflecting the structural changes during the heating and crystallization process mainly appear in the region of 1300–1100 cm^{-1} for the polyester.

Fig. 9 presents the IR spectra and the corresponding second derivatives ranging from 1100 to 900 cm^{-1}. In this range, the 1070, 1058, 986, 941 and 915 cm^{-1} bands are discerned. According to our previous study [46], the 1077 and 1058 cm^{-1} bands are probably attributed to the C–C stretching mode and the 986, 941 and 915 cm^{-1} bands to the CH_2 rocking mode. It is interesting to find that a weak peak locating at 986 cm^{-1} can be observed for the IR spectra of the PEA sample with ring-band spherulite (indicated as the arrow), while this peak can not be found in other cases. Similarly, this subtle difference is probably ascribed to the lamellar twisting during the growth of the ring-band spherulite.

From the above IR results, no remarkable difference can be identified except for the minor change that is possibly attributed to the lamellar twisting of the ring-band spherulite. So these FTIR results further indicate that the crystalline structure of PEA is not dependent on T_c and MW.

For the accurate characterization of the IR spectra, the detailed and comprehensive band assignments are essential. The major IR bands of PEA are assigned and the results are summarized in Table 3.

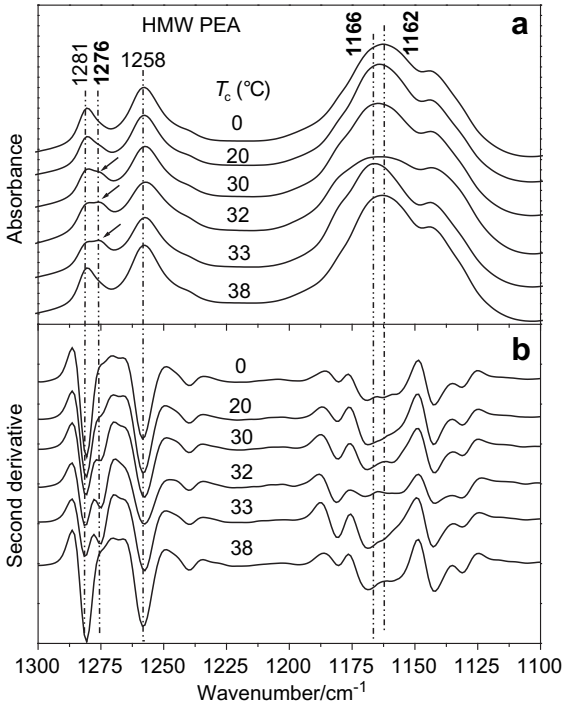

Fig. 8. (a) FTIR spectra and (b) the corresponding second derivatives in the wavenumber region of 1300–1100 cm^{-1} for HMW PEA melt-crystallized at various temperatures.

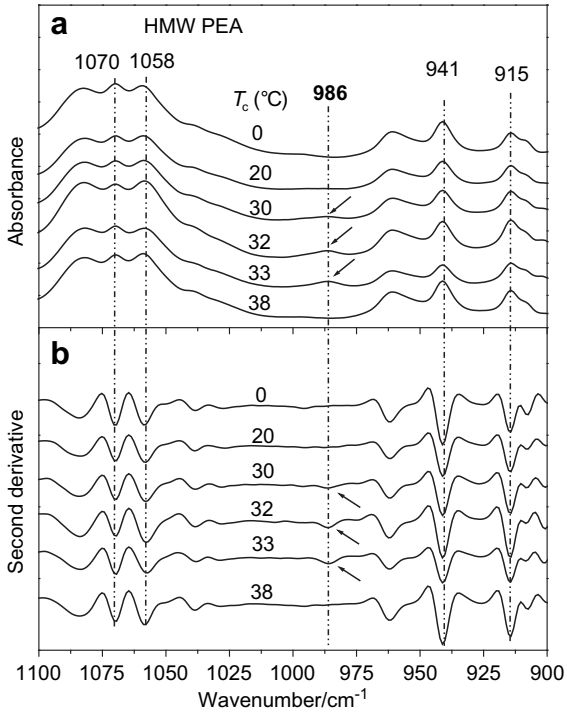

Fig. 9. (a) FTIR spectra and (b) the corresponding second derivatives in the wavenumber region of 1100–900 cm^{-1} for HMW PEA melt-crystallized at various temperatures.

3.5. In-situ FTIR analysis on isothermal crystallization

In order to follow in real-time the structural change of PEA during the isothermal crystallization process, the IR spectra ranging from 1500 to 900 cm^{-1} are collected continuously at a high crystallization temperature, 42 °C. The second derivatives at the beginning and the end of the crystallization are also shown to further identify the structural difference between the crystalline and amorphous state. Here, the temperature of 42 °C is chosen because the crystallization time at 42 °C is so long that the whole crystallization process can be followed by IR spectroscopy. Time-resolved IR spectra are shown in Fig. 10.

Fig. 10 (a) shows the second derivatives of IR spectra at the beginning (amorphous phase) and the end (crystalline phase) of crystallization at 42 °C for the HMW PEA. The time-resolved spectra are presented in Fig. 10 (b). The difference spectra calculated by subtracting the initial spectrum collected at 42 °C are depicted in Fig. 10 (c). In Fig. 10 (a), the remarkable intensity change and the band shift occur between the crystalline and amorphous phase for the IR bands, such as the 1467, 1437, 1411, 1388, 1281, 1258, 1058, 941 and 915 bands, indicating that they are crystalline sensitive bands. From parts b and c in Fig. 10, it can be clearly observed that the intensities of many IR bands increase with the time except for the 1081 cm^{-1} band. So the 1081 cm^{-1} band is ascribed to the amorphous band and the other bands are associated with the crystalline bands. In Fig. 10 (b), the crystalline bands are indicated with the arrow "↑" and the amorphous one with the arrow "↓".

The two bands at 1388 and 1162 cm^{-1}, show the distinct wavenumber shift in Fig. 10 (b), during the crystallization process at 42 °C. This can be explained as follows. During the isothermal crystallization process at a high temperature, the PEA structure may be continuously adjusted, in other words, the chain packing is progressively rearranged to form the most perfect and stable crystalline phase.

In order to investigate the crystallization kinetics of HMW and LMW PEA melt-crystallized at 42 °C by in-situ FTIR, the normalized intensity H_n of several crystalline bands (the 1467, 1258 and 941 cm^{-1} bands) as a function of crystallization time are plotted in Fig. 11. The amorphous 1081 cm^{-1} band is also shown for comparison. The 1467, 1258 and 941 cm^{-1} bands are selected as the representatives of the $\delta(CH_2)$, ν(C–O–C) and $\gamma(CH_2)$ modes, respectively. Here, H_n is defined as $(H_t - H_0)/(H_\infty - H_0)$, where H_0 and H_t respectively represent the peak height of the specific band at the beginning of the crystallization and at the crystallization time of "t", while H_∞ denotes the corresponding peak height at the end of crystallization.

The intensities of these three crystalline bands increase with time, while that of the amorphous band decreases for the HMW PEA in Fig. 11(a). It is very interesting to find that the intensity change of the 1258 cm^{-1} band is asynchronous with those of the other two crystalline bands, that is, the 1467 and 941 cm^{-1} bands. The rate of the intensity change for the 1258 cm^{-1} band is obviously

Table 3
The assignments of the major IR bands of PEA.

Wavenumber (cm^{-1})	Assignment	Wavenumber (cm^{-1})	Assignment
1467	$\delta_{as}(CH_2)$	1459	$\delta_{as}(CH_2)$
1437	$\delta_s(CH_2)$	1422	$\delta_s(CH_2)$
1411	$\delta_s(CH_2)$	1388	$\sigma_{as}(CH_2)$
1281	ν_{as}(C–O–C)	1276	ν_{as}(C–O–C), ring-band
1258	ν_{as}(C–O–C)	1166	ν_s(C–O–C), ring-band
1162	ν_s(C–O–C)	1081	ν(C–C), amorphous
1070	ν(C–C)	1058	ν(C–C)
986	$\gamma(CH_2)$, ring-band	941	$\gamma(CH_2)$
915	$\gamma(CH_2)$		

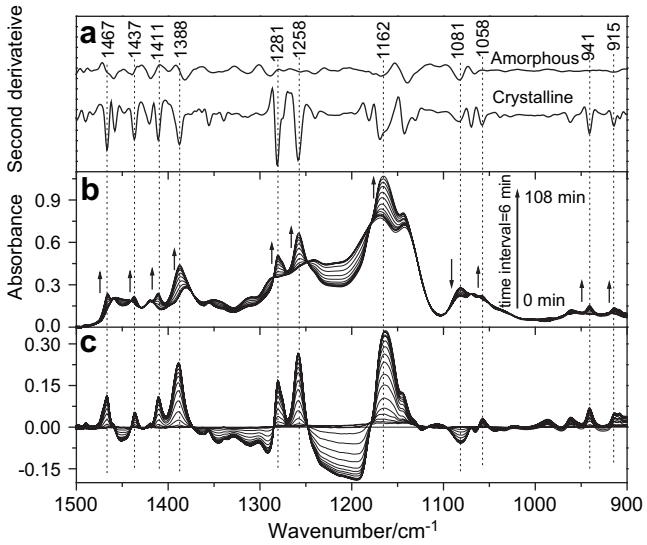

Fig. 10. (a) The second derivatives of FTIR spectra at the beginning (amorphous phase) and the end (crystalline phase) of crystallization at 42 °C for HMW PEA. (b) Time-resolved spectra of HMW PEA recorded during the isothermal crystallization at 42 °C. (c) Difference spectra calculated by subtracting the initial spectrum collected at TC = 42 °C. The arrows "↑" and "↓" indicate the crystalline and the amorphous band, respectively.

higher than those of the latter two bands. As described above, the 1258 cm^{-1} band is assigned to the ν_{as}(C–O–C) mode and the 1467 and 941 cm^{-1} bands to the $\delta_{as}(CH_2)$ and $\gamma(CH_2)$ mode, respectively. That is to say, the structural adjustment of the ester group (C–O–C) is faster than that of the C–C backbone skeleton during the crystallization process. This result is different from PBA. It is

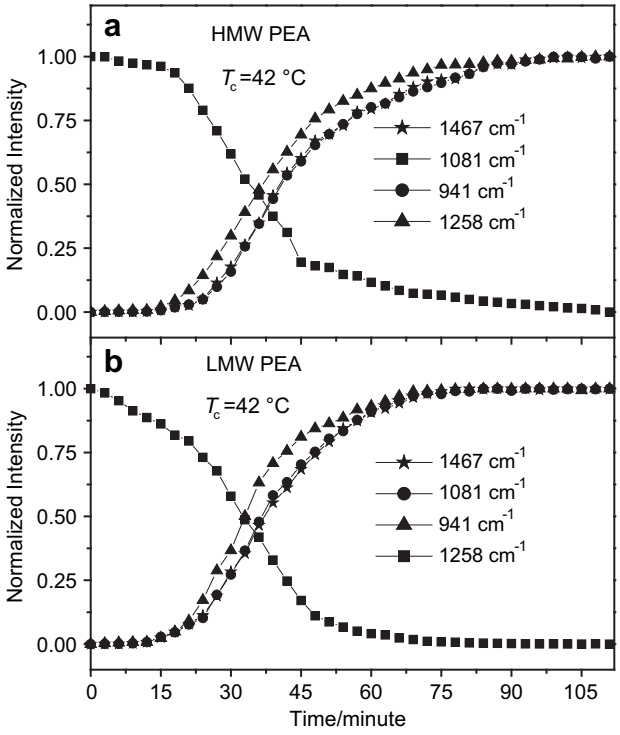

Fig. 11. Normalized peak intensity versus the time during the isothermal crystallization at 42 °C for the 1467, 1258, 1081 and 941 cm^{-1} bands in the IR spectra of (a) HMW and (b) LMW PEA.

documented [27] that the simultaneous intensity alteration of the crystalline bands occurs for PBA melt-crystallized at 48 °C. It has been reported [26,47,48] that the C–O–C and the C–C group in PHB change asynchronously with different rates and the sequential changes of these two chemical groups during the crystallization for PLLA take place. It is probably suggested that the interchain interactions precede the formation of the specific intrachain (the backbone) conformation [48]. Similarly, the same phenomenon that the structural rearrangement of the C–O–C group precedes that of the C–C backbone is found for the LMW PEA in Fig. 11(b).

When IR data are employed, the aforementioned Avrami equation can be expressed as equation (3).

$$\log\left[-\ln\left(\frac{A_t - A_0}{A_\infty - A_0}\right)\right] = \log k + n\log t \tag{3}$$

where A_t is the peak intensity of a specific crystalline band at the crystallization time t, A_0 and A_∞ denote respectively the peak intensity at the beginning and the end of the isothermal crystallization process. The $t_{1/2}$ value can be calculated with equation (2). According to equation (3), the n values of the 1258, 1467 and 941 cm^{-1} bands for the HMW PEA in the primary crystallization process are 3.11, 2.98 and 2.92, respectively, which are close to those of the PEA sample without the ring-band spherulite and lower than those with the ring-band spherulite. The n values of the corresponding 3 crystalline bands for the LMW PEA are 3.02, 3.09and 3.01. The $t_{1/2}$ values of these three bands for the HMW PEA are 36.6, 38.9 and 38.5 min, respectively. The $t_{1/2}$ values of the corresponding three bands for the LMW PEA are 32.8, 36.1 and 35.9 min, respectively. It also indicates that crystallization rates estimated from the crystalline bands for the LMW PEA are higher than those from the corresponding crystalline bands for the HMW PEA.

4. Conclusion

From the analysis of crystallization kinetics investigated by DSC, it was found that both the primary and secondary crystallization occur during the isothermal and non-isothermal crystallization process for both the HMW and LMW PEAs. The primary crystallization shows the higher n and k values than the secondary crystallization, which are associated with the confined or limited growth space in the secondary crystallization. At the same T_c or cooling rate, the LMW PEA was found to show the higher crystallization rate than the HMW PEA.

From the POM observation, it was found that depending on T_c, PEA can form the ring-band ($27 \leq T_c \leq 34$ °C) and typical Maltese-cross spherulites ($T_c < 27$ or > 34 °C). The PEA sample with the ring-band spherulite shows the larger n value than that without the ring-band spherulite. This is probably associated with the different spherulite growth mechanism.

Both WAXD and FTIR results suggested that the crystalline structure of PEA is not dependent on T_c and MW. No distinct IR spectral difference between 1500 and 900 cm^{-1} can be identified except for three bands at 1276, 1166 and 986 cm^{-1} which are ascribed to the PEA sample with the ring-band spherulite. So these three crystalline bands are the characteristic bands of the PEA samples with the ring-band spherulite. The PEA sample with ring-band spherulites shows the stronger interaction for the C–O–C group between the adjacent molecular chains. From the in-situ FTIR analysis, it was concluded that the adjustment of the ester group is faster than that of the C–C backbone and the structural rearrangements of the different chemical groups are asynchronous for PEA during the crystallization process.

References

[1] Noguchi K, Kondo H, Ichikawa Y, Okuyama K, Washiyama J. Polymer 2005;46:10823–30.
[2] Lu X, Hay JN. Polymer 2001;42:9423–31.
[3] Rybnikar F. J Polym Sci 1960;44:517–22.
[4] Woo EM, Chen JM. J Polym Sci Polym Phys Chem Ed 1995;33:1985–93.
[5] Minke R, Blackwell J. J Macromol Sci Phys 1979;B16:407–17.
[6] Minke R, Blackwell J. J Macromol Sci Phys 1980;B18:233–55.
[7] Gan Z, Abe H, Doi Y. Macromol Chem Phys 2002;203:2369–74.
[8] Gan Z, Kuwabara K, Abe H, Iwata T, Doi Y. Biomacromolecules 2004;5:371–8.
[9] Hobbs Jr SY, Billmeyer FW. J Polym Sci 1969;A-2:1119–21.
[10] Turner-Jones A, Bunn CW. Acta Cryst 1962;15:105–13.
[11] Woo EM, Wu PL, Wu MC, Yan KC. Macromol Chem Phys 2006;207:2232–43.
[12] Satoh M. Polym Prepr Jpn 2008;57:460.
[13] Zhu B, He Y, Asakawa N, Yoshie N, Nishida H, Inoue Y. Macromol Rapid Commun 2005;26:581–5.
[14] Pan P, Kai W, Zhu B, Dong T, Inoue Y. Macromolecules 2007;40:6898–905.
[15] Murayama E. Polym Prepr Jpn 2002;51:460.
[16] Woo EM, Yen KC, Wu MC. J Polym Sci Part B Polym Phys 2008;46:892–9.
[17] Pan P, Inoue Y. Prog Polym Sci 2009;34:605–40.
[18] Im SS, Kim TJ, Han S, Moon TJ, Bae YC. J Appl Polym Sci 1997;65:1745–50.
[19] Zhang F, Zhou L, Xiong Y, Xu W. J Polym Sci Part B Polym Phys 2008;46:2201–11.
[20] Supaphol P. Thermoch Acta 2001;370:37–48.
[21] Pan B, Yue Q, Ren J, Wang H, Jian L, Zhang J, et al. J Macromol Sci Part B Phys 2006;45:1025–37.
[22] Medellín-Rodríguez FJ, Larios-López L, Zápata-Espinoza A, Davalos-Montoya O, Phillips PJ, Lin JS. Marcomolecules 2004;37:1799–809.
[23] Reddy KR, Tashiro K, Sakurai T, Yamaguchi N, Sasaki S, Masunaga H, et al. Macromolecules 2009;42:4191–9.
[24] Tashiro K, Nishiyama A, Tsuji S, Hashida T, Hanesaka M, Takeda S, et al. J Phys Conf Ser 2009;184:012002.
[25] Reddy KR, Tashiro K, Sakurai T, Yamaguchi N, Hanesaka M, Sasaki S, et al. J Phys Conf Ser 2009;184:012001.
[26] Zhang J, Sato H, Noda I, Ozaki Y. Macromolecules 2005;38:4274–81.
[27] Yan C, Zhang Y, Hu Y, Ozaki Y, Shen D, Gan Z, et al. J Phys Chem B 2008;112:3311–4.
[28] Krimm S, Liang CY, Sutherlan GBBM. J Chem Phys 1956;25:549–62.
[29] Yan C, Li H, Zhang J, Ozaki Y, Shen D, Yan D, et al. Macromolecules 2006;39:8041–8.
[30] Elzein T, Nasser-Eddine M, Delaite C, Bistac S, Dumas P. J Colloid Interf Sci 2004;273:381–7.
[31] Ichikawa Y, Washiyama J, Moteki Y, Noguchi K, Okuyama K. Polym J 1995;27:1230–8.
[32] Ward IM, Wilding MA. Polymer 1977;18:327–35.
[33] Gillete PC, Dirlikov SD, Koenig JL, Lando JB. Polymer 1982;23:1759–64.
[34] Wang T, Wang H, Li H, Gan Z, Yan S. Phys Chem Chem Phys 2009;11:1619–27.
[35] Woo EM, Wu PL, Wu MC, Yan KC. Macromol Chem Phys 2006;207:2232–43.
[36] Pan P, Liang Z, Nakamura N, Miyagawa T, Inoue Y. Macromol Biosci 2009;9:585–95.
[37] Price FP. J Polym Sci Part A Polym Chem 1965;3:3079–85.
[38] Velisaris CN, Seferis JC. Polym Eng Sci 1986;26:1574–81.
[39] Woo EM, Yan SN. Polym Eng Sci 1998;38:583–9.
[40] Ren M, Song J, Zhao Q, Li Y, Chen Q, Zhang H, et al. Poly Int 2004;53:1658–65.
[41] Zhang J, Tashiro K, Tsuji H, Domb A. Macromolecules 2008;41:1352–7.
[42] Nakafuku C. Polym J 1998;30:761–3.
[43] Diaconu I, Craus M, Coman P, Caraculacu A. Rev Roum Chem 1994;39:339–46.
[44] Gazzano M, Tomasi G, Scandola M. Macromol Chem Phys 1997;198:71–80.
[45] Zhu B, He Y, Asakawa N, Yoshie N, Nishida N, Inoue Y. Macromolecules 2005;38:6455–65.
[46] Yang J, Li Z, Pan P, Zhu B, Dong T, Inoue Y. J Polym Sci Part B Polym Phys 2009;47:1997–2007.
[47] Zhang J, Tsuji H, Noda I, Ozaki Y. Macromolecules 2004;37:6433–9.
[48] Krikorian V, Pochan DJ. Macromolecules 2005;38:6520–7.